CHEMISTRY OF MATERIALS
Article

Chem. Mater. **2009,** *21,* 4993–4999 4993
DOI:10.1021/cm9026144

Low-Threshold Lasing in 3D Dye-Doped Photonic Crystals Derived from Colloidal Self-Assemblies

Shin-Hyun Kim,* Se-Heon Kim,† Woong Chan Jeong, and Seung-Man Yang*

National Creative Research Initiative Center for Integrated Optofluidic Systems and Department of Chemical and Biomolecular Engineering, Korea Advanced Institute of Science and Technology, Daejeon, 305-701 Korea. †Present address: Department of Electrical Engineering, California Institute of Technology, Pasadena, CA 91125.

Received August 25, 2009

In this article, we demonstrated low-threshold lasing in three-dimensional (3D) polymeric photonic crystals derived from colloidal suspensions. To achieve this, we used monodisperse silica beads in a photocurable refractive index matched medium with high viscosity and polarity. In this system, the colloidal silica beads rapidly self-organized into nonclose-packed fcc crystals because of strong repulsive interparticle potential relative to diminishing van der Waals attraction, and subsequently the colloid crystals were solidified by UV irradiation. Dye molecules as optical gain medium were incorporated in the polymeric matrix by simply mixing the dye molecules and the photocurable suspension before casting the photonic crystal films. The translucent composite photonic films showed emission inhibition and enhancement due to the low photon density of states (DOS) at the stop band and high DOS at the band edge, respectively. On the other hand, the porous photonic films, which were prepared by removal of silica particles from the composite films, exhibited larger bandwidth and higher reflectivity (>80%) due to the enhanced refractive index contrast. Under irradiation of excitation light source, the porous photonic film showed strongly enhanced stimulated emission at the band edge by a factor of more than 300 with respect to the spontaneous emission of dye molecules embedded in a bulk film without nanostructure. In addition, the lasing wavelength could be controlled by simply changing the particle volume fraction in the composite films from which the porous films were prepared. Moreover, the threshold excitation intensity was reduced by a factor of one-tenth relative to the previously reported values. The simple method for preparing 3D photonic crystals described here and subsequent lasing characteristics have great potential in a broad range of applications including displays, μ-TAS, and optofluidic light sources.

1. Introduction

As an alternative to the expensive top-down approach to nanoscopic structuring, self-organization of nano-building blocks has been studied intensively during the past decade in materials science and soft condensed matter physics. In particular, the self-organization of colloidal building blocks has emerged as one of the most promising and economical methods for creating 3D photonic structures, especially for the production of 3D periodic architectures with subwavelength periods.[1−3] Generally, evaporation-driven self-assembly has been used to generate close-packed colloidal crystals with face-centered cubic (fcc) or hexagonal close packing (hcp) lattices and the opaline or inverse opaline crystals exhibit photonic bandgap properties due to the periodic modulation of the dielectric constant in 3D space.[4−6] In addition, electrostatic interactions between monodisperse or bidisperse particles enable the formation of non-close-packed crystals of charged particles suspended in an aqueous phase. Depending on the type and strength of interaction as well as the particle volume fraction, various crystal lattices can be prepared.[7−13] However, the development of a simple and reliable method for fabricating practically applicable colloidal crystal devices such as photonic crystal lasers, waveguides, and sensors remains a challenge because conventional methods have

*Corresponding authors. E-mail: smyang@kaist.ac.kr, dmz@kaist.ac.kr.

(1) Wijnhoven, J. E. G. J.; Vos, W. L. *Science* **1998**, *281*, 802–804.
(2) Xia, Y.; Gates, B.; Li, Z.-Y. *Adv. Mater.* **2001**, *13*, 409–413.
(3) Vlasov, Y. A.; Bo, X.-Z.; Sturm, J. C.; Norris, D. J. *Nature* **2001**, *414*, 289–293.
(4) Jiang, P.; Bertone, J. F.; Hwang, K. S.; Colvin, V. L. *Chem. Mater.* **1999**, *11*, 2132–2140.
(5) Wong, S.; Kitaev, V.; Ozin, G. A. *J. Am. Chem. Soc.* **2003**, *125*, 15589–15598.
(6) Kim, S.-H.; Lee, S. Y.; Yi, G.-R.; Pine, D. J.; Yang, S.-M. *J. Am. Chem. Soc.* **2006**, *128*, 10897–10904.
(7) Rundquist, P. A.; Photinos, P.; Jagannathan, S.; Asher, S. A. *J. Chem. Phys.* **1989**, *91*, 4932–4941.
(8) Asher, S. A.; Holtz, J.; Liu, L.; Wu, Z. *J. Am. Chem. Soc.* **1994**, *116*, 4997–4998.
(9) Holtz, J.; Asher, S. A. *Nature* **1997**, *389*, 829–832.
(10) Monovoukas, Y.; Gast, A. P. *J. Colloid Interface Sci.* **1989**, *128*, 533–548.
(11) Yethiraj, A.; van Blaaderen, A. *Nature* **2003**, *421*, 513–517.
(12) Kim, S.-H.; Jeon, S.-J.; Yang, S.-M. *J. Am. Chem. Soc.* **2008**, *130*, 6040–6046.
(13) (a) Leunissen, M. E.; Christova, C. G.; Hynninen, A. P.; Royall, C. P.; Campbell, A. I.; Imhof, A.; Dijkstra, M.; van Roij, R.; van Blaaderen, A. *Nature* **2005**, *437*, 235–240. (b) Bartlett, P.; Campbell, A. I. *Phys. Rev. Lett.* **2005**, *95*, 128302.

Published on Web 09/24/2009

several drawbacks, including subtle fabrication conditions, the formation of intrinsic defects, and low structural rigidity.

In the present study, we demonstrate low-threshold lasing in 3D dye-doped polymeric photonic crystals derived from colloidal suspensions. To achieve this, we use monodisperse silica beads in a photocurable refractive index matched medium with high viscosity and polarity. In this system, the colloidal silica beads rapidly self-organize into non-close-packed fcc crystals (i.e., within 1 s) because of the high repulsive interparticle potential relative to the diminishing van der Waals attraction.[14,15] Our approach not only generates thin films of 3D photonic crystals over the centimeter scale in a simple and controllable manner, but also allows the easy tuning of the bandgaps and lasing wavelengths. Although many research groups have reported inhibition and enhancement of spontaneous emission of dye molecules[16−18] or quantum dots[19−21] embedded in 3D colloidal crystals or their derivatives, lasing at the band edge of colloidal crystals has been rarely reported. In particular, Shkunov et al. produced a photonic crystal laser of opaline silica structure by time-consuming slow sedimentation of silica particles.[22] Because a dye solution as an optical gain medium was infiltrated into the interstices between the silica particles, the refractive index contrast was too low resulting in long attenuation length of Bragg diffraction, and consequently the colloidal crystal was required to be relatively thick (i.e., millimeter scale). Recently, a band edge laser was demonstrated using polymerized crystalline colloidal arrays of mesoporous silica particles.[23] However, there remain still challenging issues relevant to high refraction index contrast, low threshold, high physical durability, and simple and economical fabrication processes. Other types of colloid-based lasers have also been reported; specifically, lasing in a planar resonant cavity composed of a partial mirror of colloidal crystal and a perfect mirror of dielectric stacks,[24] and lasing at a planar defect mode of colloidal crystals.[25] In both cases, dye molecules were located in the interstices either between two mirrors or in planar defect layer. Also, colloidal nanoparticle-based 1D photonic crystals were used as distributed feedback resonance cavity.[26] Our approach based on photocurable colloidal suspensions enables the fabrication of thin, high-quality photonic crystal films doped with dye molecules in a simple and inexpensive manner. In particular, our photonic crystal films templated by nonclose-packed colloidal self-assemblies are able to emit light with tunable wavelength in any location on the crystal film over a large area. The tunability of the lasing wavelength and significant enhancement of dye emission is of great importance to potential applications as disposable light sources in optofluidics and μ-TAS (total analysis system) devices.[27]

In the subsequent sections, we first described the fabrication of composite and porous photonic crystals in thin films doped with dye molecules using photocurable silica suspensions. We then discussed the emission modulation of dye molecules embedded in the composite photonic crystals. Finally, the stimulated emission of the dye molecules in the porous photonic crystals was examined to show threshold behavior and tunability of laser wavelength.

2. Experimental Section

Preparation of Dye Molecule-Embedded Photonic Crystals. Monodisperse silica particles of various sizes were synthesized through sol−gel chemistry using the Stöber−Fink−Bohn method. The silica suspensions were washed with ethanol twice and mixed with the photocurable resin, ethoxylated trimethylolpropane triacrylate (ETPTA, SR454; Sartomer) containing approximately 1 wt % 2-hydroxy-2-methyl-1-phenyl-1-propanone (HMPP, Darocur1173; Ciba Chemical) as a photoinitiator. For incorporation of dye molecules, an ethanolic solution of rhodamine B isocyanate (Aldrich) was introduced into the mixture. The ethanol was selectively evaporated from the mixture suspension in a convection oven at 70 °C for 12 h; the dye concentration in the final ETPTA suspension was 5×10^{-4} M. The resulting ETPTA suspension was cooled to room temperature and sonicated for 30 min, affording a material that showed iridescent colors attributable to the formation of a polycrystalline structure.

To obtain a film-type sample of colloidal crystals with oriented crystal planes, we inserted the suspension between two parallel glass slides separated by spacer of thickness 100 μm (polyimide tape, Kapton). The suspension was infiltrated into the gap between the plates by capillary force, and then photopolymerized by UV irradiation for 10 s. The solidified composite film was detached from the glass template and treated with 5% HF solution (50%, Sigma-Aldrich) for 12 h.

Characterization. The prepared composite and porous films were observed with an optical microscope (Nikon, L150) and reflectance spectra were measured using an optical spectrometer (Newport, OSM-100-UV-NIR) mounted on the optical microscope.

(14) (a) Kim, S.-H.; Jeon, S.-J.; Yi, G.-R.; Heo, C. J.; Choi, J. H.; Yang, S.-M. *Adv. Mater.* **2008**, *20*, 1649–1655. (b) Kim, S.-H.; Jeon, S.-J.; Jeong, W. C.; Park, H. S.; Yang, S.-M. *Adv. Mater.* **2008**, *20*, 4129–4134.
(15) Kim, S.-H.; Lim, J.-M.; Jeong, W. C.; Choi, D.-G.; Yang, S.-M. *Adv. Mater.* **2008**, *20*, 3211–3217.
(16) Martorell, J.; Lawandy, N. M. *Phys. Rev. Lett.* **1990**, *65*, 1877–1880.
(17) Lawrence, J. R.; Ying; Shim, G. H.; Jiang, P.; Han, M. G.; Ying, Y.; Foulger, S. H. *Adv. Mater.* **2005**, *17*, 2344–2349.
(18) Lopez, C.; Blanco, A.; Miguez, H.; Meseguer, F. *Opt. Mater.* **1999**, *13*, 187–192.
(19) Lodahl, P.; van Driel, A. F.; Nikolaev, I. S.; Irman, A.; Overgaag, K.; Vanmaekelbergh, D.; Vos, W. L. *Nature* **2004**, *430*, 654–657.
(20) Maskaly, G. R.; Petruska, M. A.; Nanda, J.; Bezel, I. V.; Schaller, R. D.; Htoon, H.; Pietryga, J. M.; Klimov, V. I. *Adv. Mater.* **2006**, *18*, 343–347.
(21) Garcia, P. D.; Blanco, A.; Shavel, A.; Gaponik, N.; Eychmuller, A.; Rodriguez-Gonzalez, B.; Liz-Marzan, L. M.; Lopez, C. *Adv. Mater.* **2006**, *18*, 2768–2772.
(22) Shkunov, M. N.; Vardeny, Z. V.; DeLong, M. C.; Polson, R. C.; Zakhidov, A. A.; Baughman, R. H. *Adv. Funct. Mater.* **2002**, *12*, 21–26.
(23) Yamada, H.; Nakamura, T.; Yamada, Y.; Yano, K. *Adv. Mater.* **2009**No. DOI: 10.1002/adma.200900721.
(24) Lawrence, J. R.; Ying, Y.; Jiang, P.; Foulger, S. H. *Adv. Mater.* **2006**, *18*, 300–303.
(25) Furumi, S.; Fudouzi, H.; Miyazaki, H. T.; Sakka, Y. *Adv. Mater.* **2007**, *19*, 2067–2072.
(26) Scotognella, F.; Puzzo, D. P.; Monguzzi, A.; Wiersma, D. S.; Maschke, D.; Tubino, R.; Ozin, G. A. *Small* **2009**, *5*, 2048–2052.
(27) Vezenov, D. V.; Mayers, B. T.; Conroy, R. S.; Whitesides, G. M. *J. Am. Chem. Soc.* **2005**, *127*, 8952–8953.

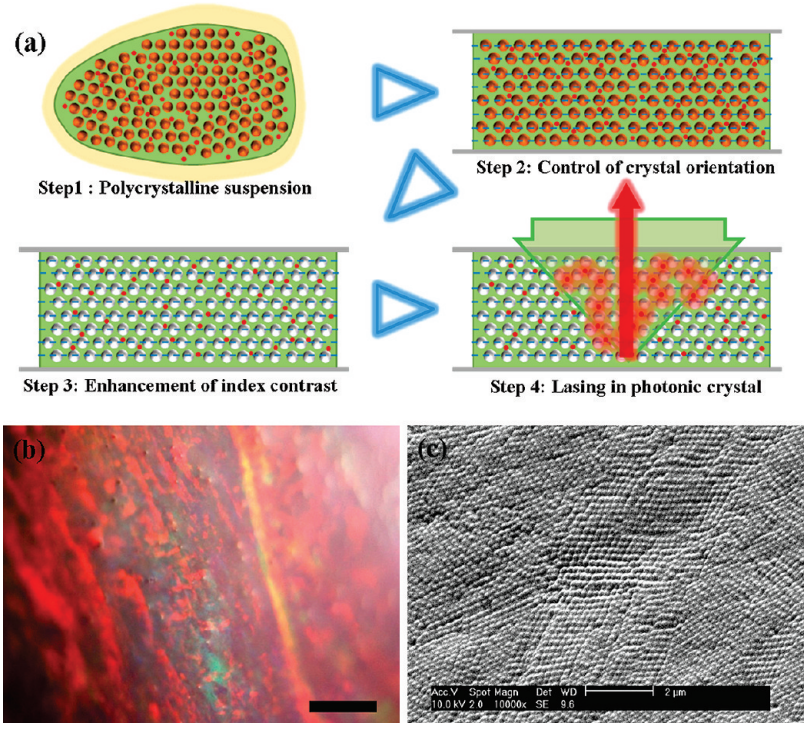

Figure 1. (a) Schematic for the preparation of porous photonic crystals with high refractive index contrasts and lasing in the photonic crystals. Confining effect of the film type geometry enables to align the (111) plane of fcc to the interface from bulk polycrystalline structures and the subsequent removal of silica particles increases the index contrast by replacing the particles with air pockets. Finally, excitation of the dye molecules embedded in polymer matrix induces the lasing action in the photonic crystals. (b) Optical microscope and (c) SEM images of the polycrystalline structure produced by bulk polymerization of silica-ETPTA suspension. The scale bars in (b) and (c) are 200 and 2 μm, respectively.

To observe the nanoscale structure of the film, a scanning electron microscope (SEM, Philips, XL30) was used. Here, the samples were coated with gold to render them conductive and typical acceleration voltages were 5−10 kV. To characterize the laser emission both above and below the threshold, a Q-switched frequency-doubled Nd:YAG laser (Quantel, Brio) emitting at 532 nm with a repetition rate of 20 Hz was used as an excitation source. A 4× objective lens was used to softly focus the pump laser beam on an area of diameter 1 mm and to collect emission signals from the films. Spectral analyses were performed by using a monochromator (Spectral Products, DK240) and a Si photo detector (New Focus, Visible Femtowatt Photoreceiver).

3. Results and Discussion

Preparation of Thin Film of Composite and Porous Photonic Crystals. To prepare high quality 3D photonic crystals for laser operation, we used silica particles dispersed in ETPTA. The fabrication processes are summarized schematically in Figure 1a. The silica particles, of ca. 200 nm in diameter, crystallized spontaneously due to the repulsive interparticle potential induced by the disjoining pressure of the solvation layer[28] and the weak electrostatic repulsion.[29] Notably, van der Waals attraction was relatively diminished because of the small index contrast between silica and ETPTA.[30] The suspensions showed iridescent colors that depended on the particle volume fraction. However, the color from the bulk crystal was not uniform. This effect is evident in Figure 1b, which shows an optical microscope image of photopolymerized colloidal crystals prepared without introducing geometrically confining templates in step 1 of Figure 1a. Multiple colors are observed because the suspended particles have a polycrystalline composite structure, which causes diffraction to occur from different crystal orientations depending on the position. Figure 1c shows a scanning electron microscope (SEM) image of surface of the polycrystalline structure, where the central region shows a square arrangement of colloidal particles (corresponding to the (100) plane of an fcc structure), whereas both sides of the image show hexagonal packing (corresponding to the (111) plane of an fcc structure). Therefore, a confining geometry is needed to control the crystal orientation, as depicted in step 2 of Figure 1a. Because colloidal crystallization commences at the wall by heterogeneous nucleation, the (111) plane of an fcc structure (the densest plane) is formed along the whole interface.[31] On the other hand, a high refractive index contrast is required to reduce the attenuation length of Bragg diffraction, which can be achieved by replacing the silica particles with air pockets, as shown in step 3. Finally, the emission of dye molecules embedded in porous photonic film was induced by irradiating with the excitation light source as shown in step 4.

(28) (a) Raghavan, S. R.; Walls, H. J.; Khan, S. A. *Langmuir* **2000**, *16*, 7920–7930. (b) Ren, J.; Song, S.; Lopez-Valdivieso, A.; Shen, J.; Lu, S. *J. Colloid Interface Sci.* **2001**, *238*, 279–284. (c) Ge, J.; Yin, Y. *Adv. Mater.* **2008**, *20*, 3485–3491.
(29) Ge, J.; He, L.; Goebl, J.; Yin, Y. *J. Am. Chem. Soc.* **2009**, *131*, 3484–3486.
(30) Jiang, P.; McFarland, M. J. *J. Am. Chem. Soc.* **2004**, *126*, 13778–13786.
(31) Grier, D. G.; Murray, C. A. *J. Chem. Phys.* **1994**, *100*, 9088–9095.

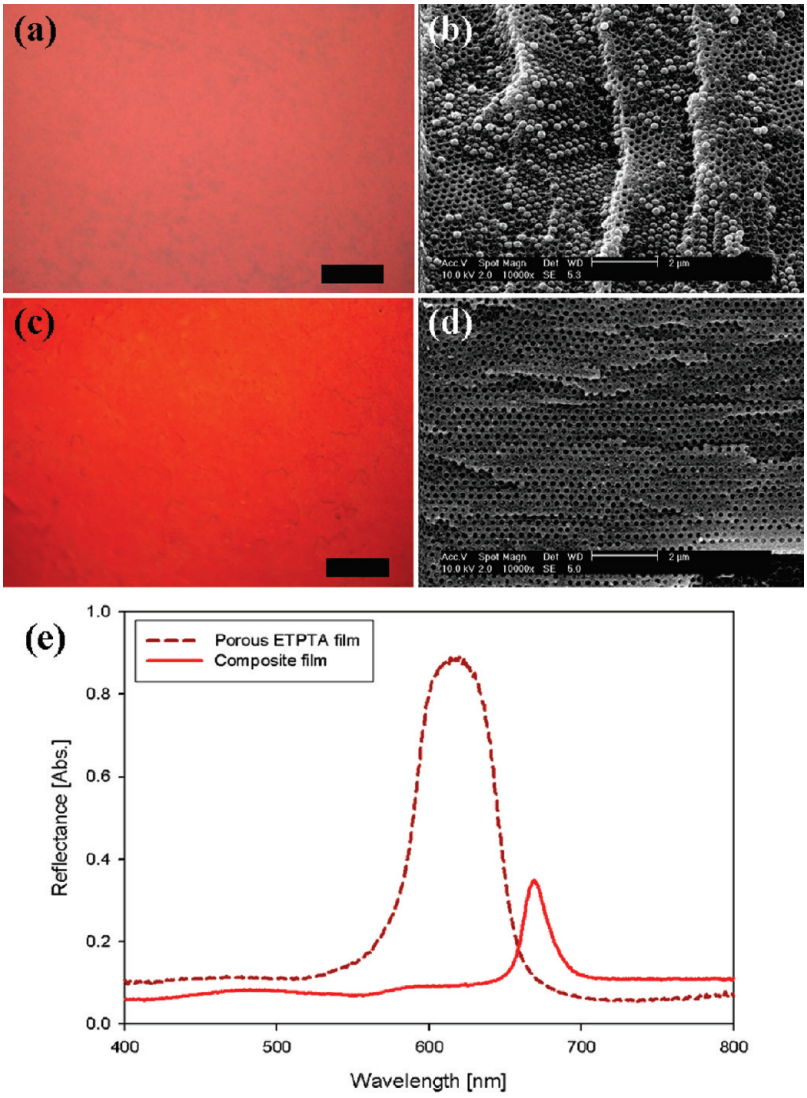

Figure 2. Optical microscope and SEM images of (a, b) the composite and (c, d) porous photonic crystals, respectively. Optical microscope images display the color of film surfaces while SEM images show particle or pore arrays on cross sections of the films. (e) Reflectance spectra of the composite and porous photonic crystal films. Here, the suspension with 207 nm silica at $\phi = 0.3$ was used. The scale bars in (a, c) and (b, d) are 200 and 2 μm, respectively.

As a confining geometry, we employed a planar gap between two glass slides separated by 100 μm with a transverse dimension of a few centimeters. The gap was infiltrated completely within 10 min with ETPTA suspension of 207 nm silica particles at a volume fraction (ϕ) of 0.3 by capillary force and the suspension was photopolymerized under UV irradiation for 10 s, which induced solidification of the structure. The resulting 100 μm thick composite films were translucent because the refractive index of silica particles ($n_{silica} = 1.45$) nearly matches that of ETPTA ($n_{ETPTA} = 1.4689$). However, the films reflect a vivid red color when exposed to normal incident white light. The optical microscope image in Figure 2a shows a uniform red color through the surface and the corresponding reflectance spectrum denoted as a solid line in Figure 2e had a maximum at 668 nm and a full width at half-maximum (fwhm) of 20 nm. The reflective color and spectrum observed under a normal incident beam arise because of constructive interference of reflected lights by stacked (111) planes. The wavelength λ of maximum peak can be estimated using Bragg's equation

$$\lambda = 2dn_{eff} = \left(\frac{\pi}{3\sqrt{2}\phi}\right)^{1/3}\left(\frac{8}{3}\right)^{1/2} D(n_p{}^2\phi + n_m{}^2(1-\phi))^{1/2} \quad (1)$$

where D is the particle diameter, and n_p and n_m denote the refractive indices of the particles and matrix, respectively. Equation 1 assumes a constant interparticle distance between all nearest neighbors at a given volume fraction. Although the composite film displays only flat ETPTA surface without exposing arrays of silica particles due to repulsion between silica and glass wall, a cross-section of the composite film shows a nonclose-packed colloidal crystalline structure, as shown in Figure 2b. Dimples in the cross-sectional SEM image of Figure 2b were left behind by the detached silica particles during fracture. Also, a cross-sectional SEM image at lower magnification was included in Figure S1a of the Supporting Information.

To increase the index contrast, thereby increasing the reflection intensity and width of the stop band, we removed the silica particles from the composite film by selective wet etching. Although the silica particles were isolated within the ETPTA matrix, they could be dissolved and removed outside of the ETPTA matrix through small pores in the cross-linked polymer network with treatment of HF solution for 12 h.[13,14] This treatment yielded opaque porous films with a high reflectivity of 90% at the stop band. Figures 2c and 2d show an optical microscope image of the porous film and an SEM image of the cross-section, respectively. In Figure S1b of the Supporting Information, we displayed a cross-sectional SEM image at lower magnification. The reflectance spectrum from the porous film exhibited a maximum peak at 618 nm with a fwhm of 57 nm (dotted line in Figure 2e). The blue-shift of the stop band and increase in the bandwidth were caused by a decrease in the effective refractive index and an increase in the index contrast, respectively.

As an optical gain medium, we introduced dye molecules into the polymeric matrix by mixing 5×10^{-4} M rhodamine B isocyanate with the ETPTA suspension before infiltration into the gap. The dye concentration was carefully chosen so as to be small enough not to influence the colloidal crystallization but large enough to generate sufficiently strong photoluminescence (PL) emission for lasing even after photopolymerization of ETPTA. Figure 3 shows optical images of typical composite and porous photonic films doped with dye molecules. As noted, both of the photonic films were freestanding and amenable due to high physical rigidity due to high cross-linking density of the ETPTA matrix. As can be noted in Figure 3a, the composite film is translucent due to index matching between the colloidal particles and matrix; in this image, the bright red strip is caused by Bragg diffraction and the weak red color observed over the entire film is due to the doped dye molecules. The color of the strip due to Bragg diffraction can be changed by varying the angle of incidence of the light beam as shown in the inset of Figure 3a. The porous film, by contrast, is opaque because of its higher index contrast and shows a much brighter reflection color with a metallic luster, as shown in Figure 3b and its inset.

Emission Modulation of Dye Molecules in Composite Photonic Crystals. We first describe the excitation results of the composite photonic films. To excite the rhodamine B isocyanate embedded in composite photonic film, we used a frequency-doubled Q-switched Nd:YAG laser emitting at 532 nm with a repetition rate of 20 Hz. The laser beam was focused on the surface of the film with an irradiation spot of diameter 1 mm, using a 4× objective lens. Emission from the film was collected by the same objective lens and the spectrum was analyzed using a monochromator and a photodetector. As we described in eq 1, the particle volume fraction determines the interparticle distance and consequently the bandgap position due to repulsive interparticle interaction. By using three volume fractions (ϕ = 0.43, 0.42, and 0.40) while keeping the silica particle size constant at 200 nm, we obtained

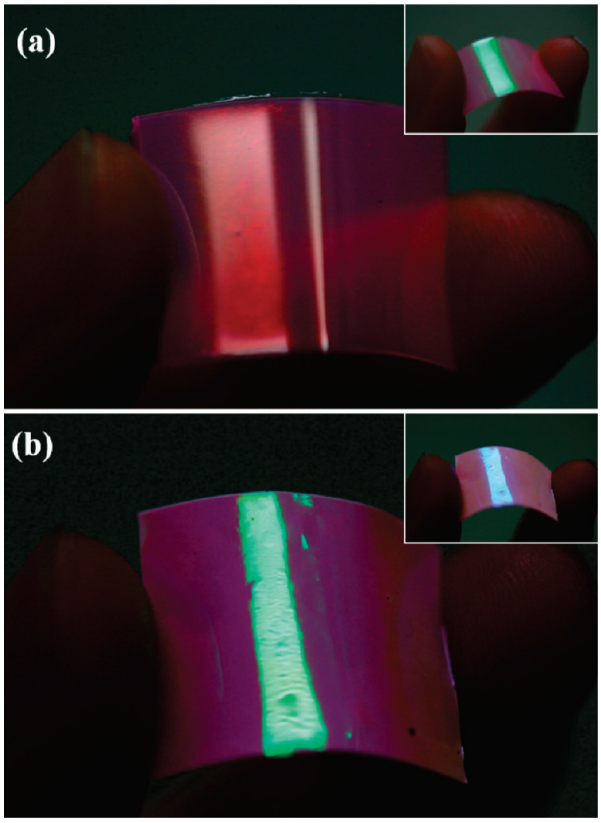

Figure 3. Images of (a) composite and (b) porous films of photonic crystals. The insets were taken at different angles.

three different stop band positions of λ = 573, 578, and 585 nm, respectively, as denoted in Figure 4a. Because these stop band positions are well within the emission spectrum of rhodamine B isocyanate embedded in bulk ETPTA, it is expected that the original spontaneous emission spectrum of the dye molecules would be modified at the stop band position.[16,17] When irradiated with an excitation intensity of 2 MW/cm^2, the PL spectra show clear features of inhibition of spontaneous emission at the respective stop band positions and enhancement at the band edges (Figure 4b). According to Fermi's golden rule, the emissive transition rate of an atomic emitter should be proportional to the DOS. Thus, the extremely low DOS at the stop band position and high DOS at the band edges will suppress and promote emissive transitions of the dye molecules at these wavelengths, respectively. When a higher excitation intensity was used from 2.47 to 8.87 MW/cm^2, the emission spectra did not show any noticeable change as shown in Figure 5. It means that the dye molecules doped in the composite film did not show stimulated emission or threshold behavior and lasing could not be achieved in the composite films.

Lasing in Porous Photonic Film. Now we consider the porous photonic films. Because the removal of the silica particles from the composite films results in a strong blue-shift of the stop band position with respect to the emission spectrum of rhodamine B isocyanate, we prepared suspensions of smaller volume fractions containing larger particles to locate the photonic band edge of the porous photonic film near the gain spectrum. The porous films

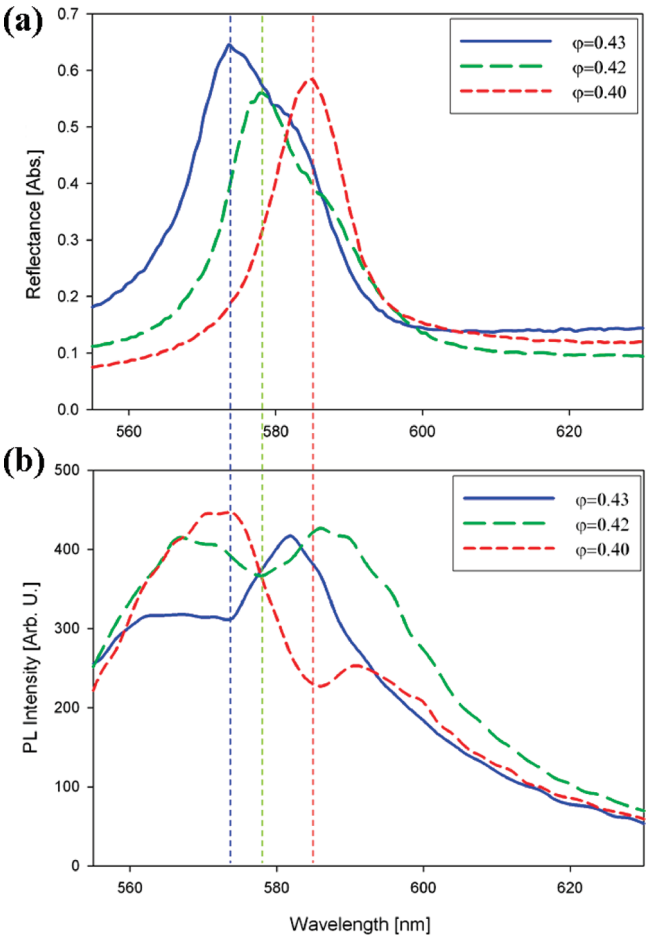

Figure 4. (a) Reflectance and (b) PL spectra of three composite photonic crystal films with different stop band positions. At the wavelength of the maximum reflectance, the PL of rhodamine B isocyanate was inhibited and showed a dip. Here, three composite films were composed of 200 nm silica particles of three different particle loadings $\phi = 0.43$, $\phi = 0.42$, and $\phi = 0.40$.

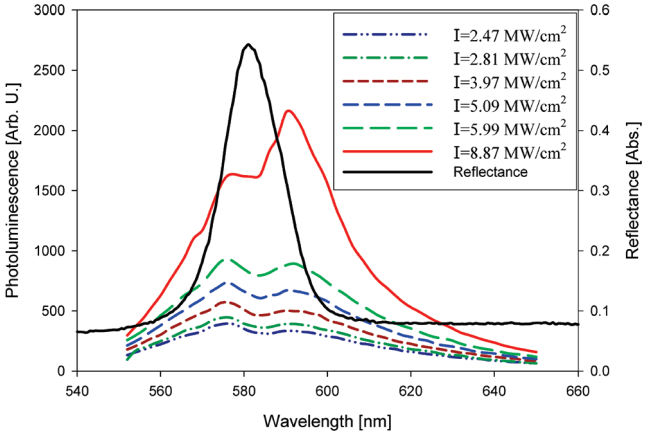

Figure 5. PL and reflectance spectra from the composite film. Dips at the bandgap positions were observed under various excitation intensities.

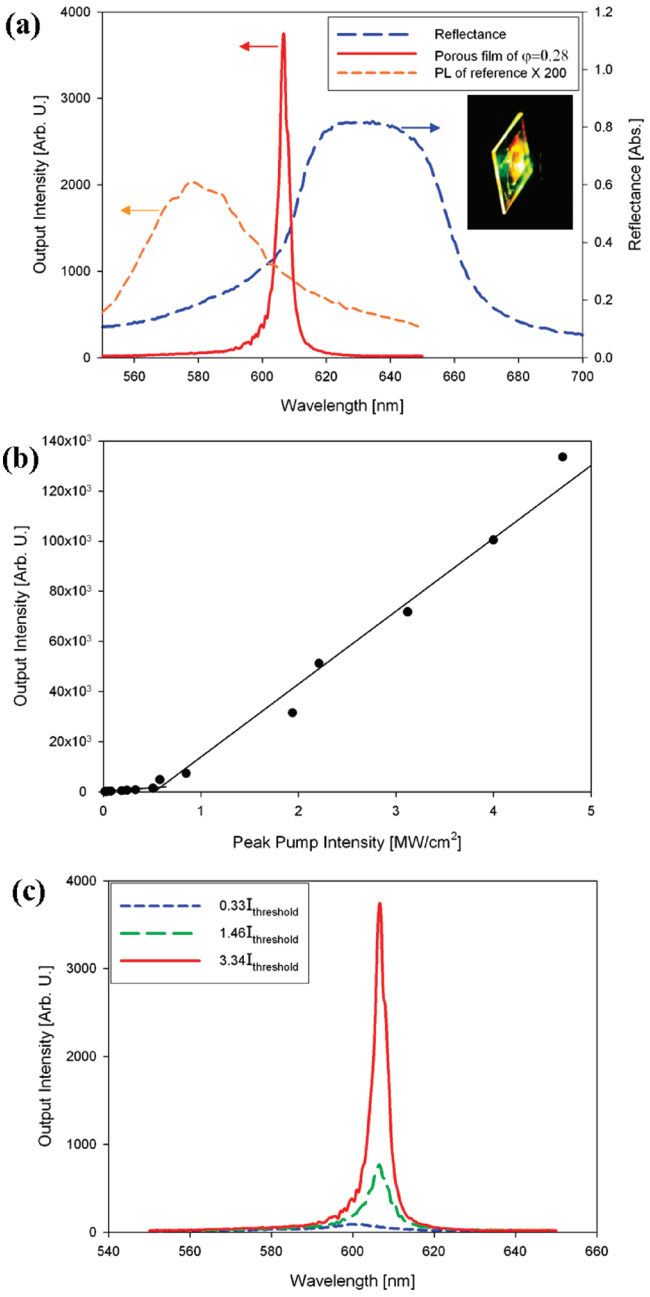

Figure 6. (a) Emission and reflectance spectra of rhodamine B isocyanate-doped porous photonic film. The dotted orange line is the PL spectrum from the rhodamine B isocyanate-embedded bulk ETPTA film without nanostructure. Here, the intensity of the bulk film is multiplied by 200 for a clear comparison. Inset of (a) is the optical image of porous photonic crystal film irradiated with excitation laser source. (b) A typical $L-L$ (light-in versus light-out) curve shows threshold characteristics of the laser, from which the threshold is estimated to be 0.6 MW/cm^2. (c) Emission spectra from the rhodamine B isocyanate-embedded porous photonic film under three different excitation intensities. The measured linewidths (fwhm) under excitation intensities of $0.33I_{\text{threshold}}$, $1.46I_{\text{threshold}}$, and $3.34I_{\text{threshold}}$ are 25, 8, and 3.5 nm, respectively. Here, the porous films were derived from the composite film with 207 nm silica particles at $\phi = 0.28$.

were fabricated by first preparing composite films composed of 207 nm silica particles at $\phi = 0.28$, and then removing the particles by wet etching. The resulting porous photonic films had a stop band at 633 nm. As shown in Figure 6a, the reflectance spectrum showed more than 80% reflectivity at the maximum and a fwhm of 51 nm, indicating that the porous crystal was of high quality. When the porous film was irradiated by the excitation laser, the emission spectrum differed from that of the dye-doped bulk ETPTA film without nanostructure (denoted as the reference) in three key aspects: (1) the emission line width was narrowed from 45 to 3.5 nm; (2) the peak emission wavelength was red-shifted from

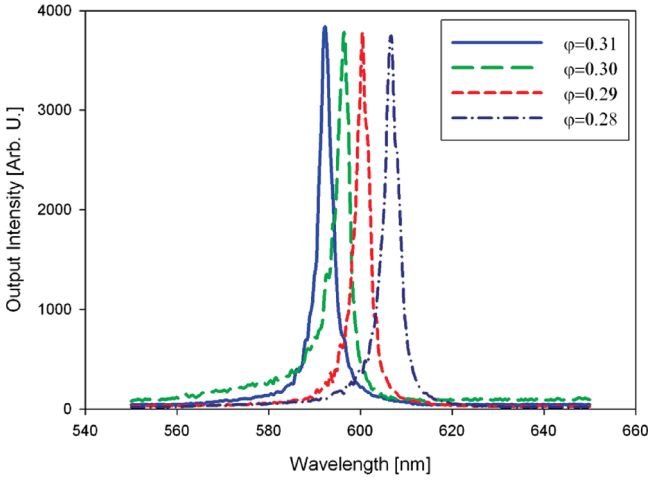

Figure 7. Emission spectra from four porous films with different stop band positions. Here, four porous films were derived from the composite films with 207 nm silica particles at different particle loadings $\phi = 0.31$, $\phi = 0.30$, $\phi = 0.29$, and $\phi = 0.28$.

578 to 606 nm, which traces the upper band edge position; and most importantly, (3) the peak emission intensity was enhanced by a factor of more than 300. These distinctive characteristics are due to stimulated emission at the band edge of the porous photonic film. The inset of Figure 6a shows an optical image of the porous photonic film irradiated with light of wavelength 532 nm using the frequency-doubled Nd:YAG laser. Here, the greenish color originates from the excitation laser, whereas the bright orange color indicates laser emission from the dye molecules.

Additional studies were performed to further elucidate the observed lasing action. To show the threshold behavior, which is a typical characteristic of lasers, we measured a light-in versus light-out ($L-L$) curve using neutral density filters of various transmittances as a means of generating various excitation intensities. Figure 6b and 6c show $L-L$ curve and the PL spectra obtained using various excitation intensities, respectively. From Figure 6b, we determined the threshold excitation intensity to be 0.6 MW/cm^2, which is lower by a factor of 1 tenth than the previously reported values for dye solution-infiltrated opal structures and polymerized crystalline colloidal arrays of mesoporous silica particles.[22,23]

To tune the laser emission wavelength, we prepared porous films with different bandgap positions by removing the silica particles from composite structures with different volume fractions of $\phi = 0.31$, 0.30, 0.29, and 0.28. Using these porous films, we successfully tuned the laser wavelength to 593, 597, 601, and 606 nm, respectively, as shown in Figure 7.

4. Conclusions

We demonstrated a simple and controllable method for the preparation of composite and porous photonic films by infiltrating a photocurable colloidal suspension into the gap between two parallel glass plates and then solidifying the matrix by UV irradiation. Films doped with dye molecules as optical gain medium showed emission inhibition and enhancement phenomena due to the low DOS at the stop band and high DOS at the band edges. Especially, the porous films with high index contrast showed strongly enhanced stimulated emission at the band edge by a factor of over 300 with respect to the spontaneous emission of dye molecules embedded in a bulk film without nanostructure. In addition, the lasing wavelength could be controlled by simply changing the volume fraction of particles in the composite films from which the porous films were prepared. The simple and novel method for preparing 3D photonic crystals in low cost and subsequent lasing or emission modulation will be useful in a broad range of photonic applications including displays, optical switches, and disposable light sources in μ-TAS and optofluidic systems.

Acknowledgment. This work was supported by a grant from the Creative Research Initiative Program of the Ministry of Education, Science and Technology for "Complementary Hybridization of Optical and Fluidic Devices for Integrated Optofluidic Systems." The authors also appreciate partial support from the Brain Korea 21 Program.

Supporting Information Available: SEM images to show the cross-sectional images of the composite and porous films at low magnifications (PDF). This material is available free of charge via the Internet at http://pubs.acs.org.